Available online at www.sciencedirect.com
SCIENCE DIRECT®
International Journal of Solids and Structures 42 (2005) 637–645
INTERNATIONAL JOURNAL OF SOLIDS and STRUCTURES
www.elsevier.com/locate/ijsolstr

Nano-ductile crack propagation in glasses under stress corrosion: spatiotemporal evolution of damage in the vicinity of the crack tip

S. Prades, D. Bonamy *, D. Dalmas, E. Bouchaud, C. Guillot

Groupe Fracture, Service de Physique et Chimie des Surfaces et Interfaces, DSM/DRECAM/SPCSI, CEA-Saclay, F-91191 Gif sur Yvette, France

Received 19 April 2004
Available online 10 August 2004

Abstract

Recent experiments have evidenced the existence of a ductile fracture mode at the nanometer scale in Aluminosilicate glass. The present study is designed to check whether such a ductile mode is inherent to the amorphous nature of glass. Therefore, the slow crack advance is observed in real time via an Atomic Force Microscope in a *minimal* glass, amorphous Silica, under stress corrosion. In this case, the Crack propagation proceeds by the nucleation, growth and coalescence of damage cavities as in the Aluminosilicate glass, but the cavity size is significantly larger. We focus here on the kinematics of crack propagation by looking at the spatio-temporal evolution of both the tip of the main crack and the cavity ahead. It is shown that the velocity of the main crack tip is significantly lower than the one of the cavity edge toward the main crack tip, like in metallic alloys. Moreover, the velocities of the different fronts (main crack, frontward and backward cavity tips) at these nanometric scales is one order of magnitude smaller than the crack tip velocity at the continuum scale. This has important consequences for the modelling of stress corrosion, especially at ultra-slow crack propagation.

PACS: 62.20.Mk; 81.40.Np; 87.64.Dz
Keywords: Fracture and cracks; Corrosion fatigue; Brittleness; AFM

* Corresponding author. Tel.: +33 1 69 08 21 14; fax: +33 1 69 08 84 46.
E-mail address: bonamy@drecam.cea.fr (D. Bonamy).

0020-7683/$ - see front matter © 2004 Elsevier Ltd. All rights reserved.
doi:10.1016/j.ijsolstr.2004.06.024

1. Introduction

It is often thought that brittle fracture in glass proceeds like in cleavage, by successive breaking of atomic bonds, and does not involve any damage occurring ahead of the crack tip. On the contrary, it is well known that ductile fracture of metallic alloys involves the nucleation, growth and coalescence of damage cavities (see for instance Pineau et al., 1995). In these cases, nucleation usually occurs at microstructural ''defects'', such as second phase precipitates unable to accommodate plastic deformation. Then, the voids grow under the action of the stress triaxiality (Rice and Tracey, 1969), and blunt when extending into the metallic matrix. Such a mechanism leads to rough fracture surfaces, which have been extensively described using fractal geometry (Mandelbrot et al., 1984; Bouchaud, 1997). If observed at the scale of some tens or hundreds of micrometers, with an optical microscope for example, glass fracture surfaces may appear mirror-flat. However, when observed with an atomic force microscope (AFM), they exhibit a morphology very similar to the one of metallic alloys, but at length scales several orders of magnitude smaller (Daguier et al., 1997).

Furthermore, it was shown (Guilloteau et al., 1996; Hénaux and Creuzet, 2000) that in the vicinity of the crack tip, deformations do not fit with a linear elastic description, which is also an observation commonly made in the field of metallic materials.

These puzzling similarities between metallic alloys and glasses suggest a similarity in the fracture modes of these two types of materials. As a matter of fact, Molecular Dynamic (MD) simulations have predicted that a main crack triggers in a glass the growth of cavities nucleated from regions of more stretched Si–O bonds, *intrinsically* linked to the amorphous structure (Van Brutzel, 1999; Van Brutzel et al., 2002; Rountree et al., 2002). These cavities subsequently grow under the action of the local stress field, and finally merge with the main crack, which is then able to progress by a distance comparable to the length of the cavities.

These various results have led us to analyze the fracture mode of glass with an AFM, which provides the relevant length scales of observation (1 nm–10 μm). In order to follow the crack propagation in situ, we had to study very slow fractures, and we have grown sub-critical stress corrosion (Wiederhorn, 1967; Wiederhorn and Bolz, 1970; Lawn, 1993) mode I cracks.

The first series of experiments were reported in Célarié et al. (2003a,b) and Marlière et al. (2003): the growth and coalescence of damage cavities in an aluminosilicate glass were observed via an AFM. It has been shown that the non-linear elastic behaviour (Célarié et al., 2003a) actually occurs in the damaged zone containing the cavities, ahead of the crack tip.

We report here new experiments performed on pure amorphous silica. Both our experimental set-up and protocol are described in Section 2. In Section 3, we present the experimental results, and we focus on the interaction between the main crack tip and the first cavity ahead (Section 4). The cavity progresses up to the crack tip, which moves significantly slower than the cavity edge, and this behaviour is compared to what happens in metallic alloys. The merging of the cavity with the main crack induces a jump in the crack velocity, which on average is one order of magnitude larger than the main crack velocity prior to coalescence. Finally, Section 5 is devoted to a discussion on the mechanisms of cavity extension, in relationship with the post-mortem morphology of fracture surfaces and with the intermittency of crack propagation, as observed at various length scales.

2. Experimental set-up

The experimental set-up is shown in Fig. 1. Two symmetrical cracks are initiated on DCDC (double cleavage drilled compression) parallepipedic samples of pure silica glass (see Fig. 1a). All the experiments

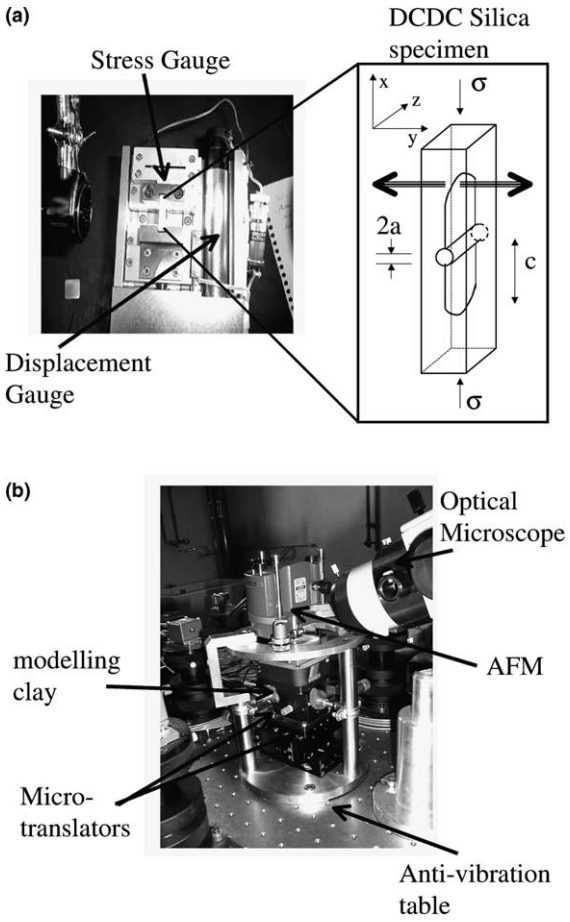

Fig. 1. Experimental set-up: (a) loading configuration used to fracture the glass sample via stress corrosion; (b) system of observation.

were performed in the room atmosphere, during a period (around one month) while the relative humidity and the temperature were $45 \pm 3\%$ and 26.0 ± 2 °C respectively.

We have chosen to investigate a very simple material, pure silica glass, to evaluate the influence of the glass structure by comparing the present results to those obtained on a complex aluminosilicate with lithium (Célarié et al., 2003a,b; Marlière et al., 2003).

The size of the specimens is $5 \times 5 \times 25$ mm^3, and the 5×25 mm^2 surfaces are optically polished (RMS roughness is 0.25 nm for a 10×10 μm scan size). In the center of the two parallel 5×25 mm^2 surfaces, and perpendicularly to them, a cylindrical hole (radius $a = 0.5$ mm) is drilled. Its axis defines the z-direction. The x-axis (respectively the y-axis) is parallel to the 25 mm (respectively the 5 mm) long side of the 5×25 mm^2 surfaces (Fig. 1a).

A uniaxial compressive load is applied perpendicularly to the 5×5 mm^2 surfaces. The external stress σ is gradually increased through the slow constant displacement (0.01 mm/min) of the grips. Once the two cracks (which progress symmetrically from the hole) are initiated, the displacement of the grips is stopped. The two crack fronts then propagate symmetrically along the x-axis in the symmetry plane of the sample, parallel to the (x, z) plane (fracture plane). In this geometry, the stress intensity factor K_I is given by (He et al., 1995)

$$K_I = \frac{\sigma\sqrt{a}}{0.375c/a + 2} \tag{1}$$

where c is the length of one of the two cracks (see Fig. 1a). The cracks first propagate very quickly. In this dynamical regime, the crack velocity v is supposed to be independent of the environment. But, as the crack length c increases, the stress intensity factor K_I decreases (Eq. (1)), to finish up being lower than the fracture toughness K_{Ic}. Under vacuum the cracks would then stop. But, in a humid atmosphere, the corrosive action of water on glass allows a slow, sub-critical, cracks propagation. The crack tip advance is then slow enough to be monitored by our apparatus represented in Fig. 1b: For velocities v ranging from 10^{-6} to around 10^{-9} $m\,s^{-1}$, optical images recorded by a digital camera allow to determine the crack tip position as a function of time, and consequently to determine the mean velocity. For velocities lower than 10^{-9} $m\,s^{-1}$, the crack tip position is determined using AFM frames at relatively high magnifications (scan sizes ranging from 5×5 μm^2 to 500×500 nm^2).

From the knowledge of the crack length c and the load σ, one can deduce K_I (Eq. (1)). Fig. 2 presents the variation of the mean crack tip velocity v as a function of the stress intensity factor K_I. The exponential behaviour is compatible with stress enhanced activated process models (Wiederhorn, 1967; Wiederhorn and Bolz, 1970; Célarié et al., 2003b).

Using this graph, it is now possible to set the average crack tip velocity by adjusting the external applied load for a measured crack length. The protocol is the following: First, a large load is applied to reach a velocity close to 10^{-8} $m\,s^{-1}$. Second, the load is decreased to a value *inferior to* the prescribed one. Finally, the load is increased again up to the value that corresponds to the prescribed velocity. The force is then fixed to this value and the evolution of the crack tip is immediately followed by AFM. This procedure allows us to get clearly separated velocity zones, with "new" crack tips with minimal corrosion ageing at the beginning of each of these zones (see also Guin and Wiederhorn, 2003 for related discussion). Furthermore, this procedure allows us to orient the play in the compressive machine always in the same direction.

In situ AFM observations of the crack tip vicinity are thus performed for prescribed very low velocity values (10^{-9} to 10^{-13} $m\,s^{-1}$). In the following, we present experimental results for a mean velocity of 4×10^{-11} $m\,s^{-1}$, and we focus our attention on the dynamical aspects of the first cavity ahead of the crack tip.

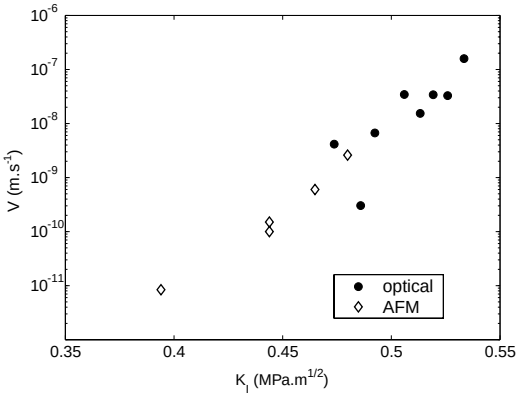

Fig. 2. Variation of the continuous crack tip velocity v (in $m\,s^{-1}$) as a function of the stress intensity factor (in $MPa\,nm^{1/2}$). The black points correspond to optical measurement and the diamonds correspond to AFM measurements.

3. In situ observations

Fig. 3 presents nine successive AFM topographic frames in the vicinity of the crack tip in the pure silica glass sample. Each scan is recorded at a recording rate of 3 Hz (at this frequency, a scan is obtained in about 3 min). The crack propagates along the x axis at an average velocity of 4×10^{-11} m s^{-1}. The frames size is 470×135 nm^2 and the height range is 3 nm.

Fig. 3b reveals a depression ahead of the crack tip of typically 100 nm in length and 25 nm in width, which is shown, using FRASTA method, to be a damage cavity (Célarié et al., 2003a; Kobayashi and Shockey, 1987). This cavity grows with time (Fig. 3b–f) until reaching a length of about 150 nm. Then the cavity coalesces with the crack tip (Fig. 3g–h) before advancing through all the area of observation via the coalescence with an other hidden cavity ahead. The kinematics of cavity growth is analyzed in the next section.

4. Kinematics of the various fronts during the growth and coalescence of cavities

In order to investigate the precise kinematics of crack propagation, we have plotted the spatiotemporal diagram of the evolution of the crack line as recorded in the sequence represented in Fig. 3. The method is the following: First, the crack line is determined on the last frame of the sequence that shows the crack path once the area of observation has been entirely crossed by the crack (dark arrow in Fig. 4a). Then, the *same* line is taken from each frame of the entire sequence, which contains 150 frames although Fig. 3 represents only nine of these frames, and sorted chronologically. The resulting spatiotemporal diagram is represented in Fig. 4b.

The temporal evolution of the various fronts is then determined by extracting contours of constant height z from the previous spatiotemporal diagram. The contour corresponding to $z = -0.8$ nm is represented in Fig. 5. The time evolution of the main crack tip (CT), of the forward front tip (FF) and the backward front tip (BF) of the cavity can then be deduced. For each one of these three fronts, the mean velocity $\langle v \rangle$ is defined as the average of the slopes of the linear fits of contours taken at 20 different constant heights. These average velocities are equal to $\langle v \rangle^{CT} = 4 \times 10^{-12}$ m s^{-1}, $\langle v \rangle^{FF} = 1.1 \times 10^{-11}$ m s^{-1} and $\langle v \rangle^{BF} = 1.2 \times 10^{-11}$ m s^{-1} for the main crack tip, the forward front tip and the backward front tip of the cavity, respectively. All these velocities are significantly smaller than the mean crack tip velocity $v = 4 \times 10^{-11}$ m s^{-1}

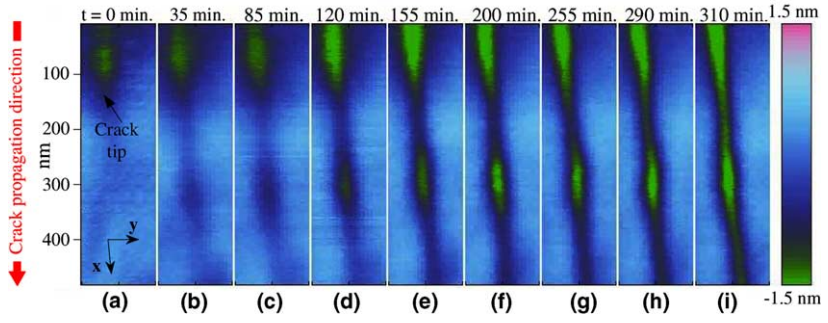

Fig. 3. Sequence of topographic AFM frames (470×135 nm^2) in the vicinity of the crack tip, showing the propagation of a mode I crack along the x-axis. (a,b) apparition of a nanometric damage cavity ahead of the crack tip, (c–f) growth of the cavity prior to crack propagation and (g,h) coalescence of the cavity with the main crack, (i) the crack has advanced through all the observable part of the sample.

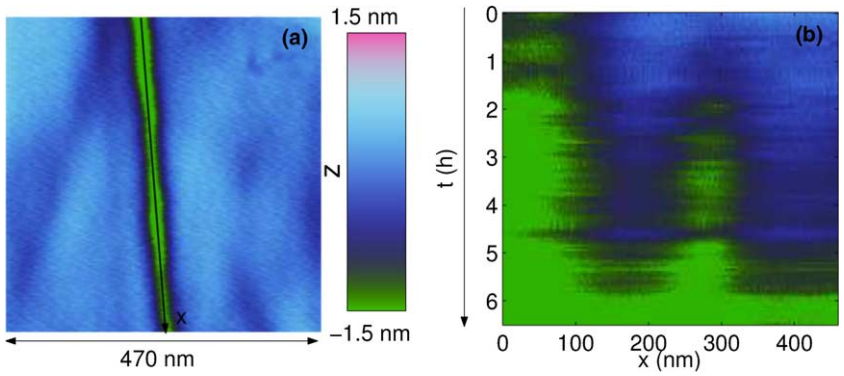

Fig. 4. (a) Last frame of the sequence presented in Fig. 3 showing the crack line (black arrow $\vec{x}$) at the surface of the specimen once the crack went through the area of interest. (b) Spatiotemporal diagram of the evolution of this line. Each row i of this image shows the topography profile, given by the color of the pixel according to the colorbar shown between figure (a) and (b), along the direction $\vec{x}$ of the frame i of sequence. The last row of this diagram thus represents the topography of the black line in figure a. At the continuum scale, the crack propagates from left to right (along the x-direction). Time increases from top to bottom.

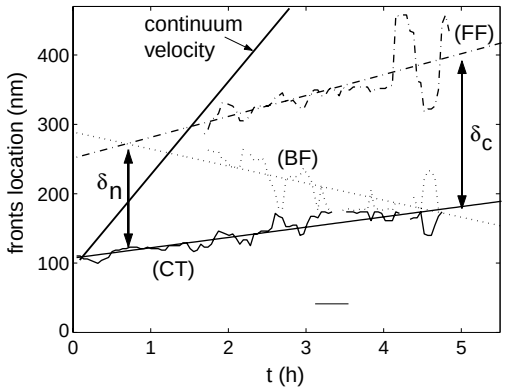

Fig. 5. Temporal evolution of the main crack front (CT) (plain) and the back (BF) (dot) and front (FF) (dash–dot) of the cavity. The average velocities of these fronts are determined through linear fits, the various straight lines. The intersections of these lines allow us to define the distance δ_n between the main crack tip and the nucleation point and the size δ_c of the cavity at coalescence. The thicker line shows the velocity at the continuum scale.

measured at the continuous scale. At these nanometric scales, the main crack front does not propagate regularly, but intermittently through the merging with the nanoscale cavities (Fig. 6).

The tip positions of any of these three fronts fluctuate rather widely on both sides of the linear fits. As a matter of fact, the standard deviations are $\sigma_v^{CT} = 1 \times 10^{-12}\ \mathrm{m\,s^{-1}}$, $\sigma_v^{FF} = 7 \times 10^{-12}\ \mathrm{m\,s^{-1}}$ and $\sigma_v^{BF} = 1.1 \times 10^{-11}\ \mathrm{m\,s^{-1}}$ for the main crack tip, the forward front tip and the backward front tip of the cavity respectively, i.e. they are of the same order of magnitude as the average value of the velocity. The motion of these three fronts is extremely correlated. This indicates a strong coupling between the forward/backward movement of the main crack tip and the increase/decrease of the cavity size.

One can extrapolate the spatiotemporal location of the cavity nucleation from the crossing point of the linear fits of FF and BF (Fig. 5). Similarly, the coalescence time and location is defined as the point where the linear fits of CT and BF intersect (Fig. 5). From these intersections, one can deduce the distance δ_n separating the main crack tip and the nucleation point, and the size δ_c of the cavity at coalescence. These two

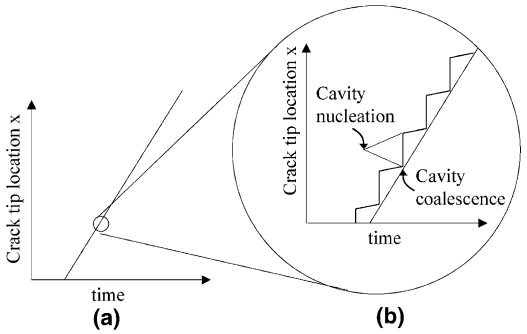

Fig. 6. Sketch of the crack tip propagation at (a) the macroscopic scale and (b) the cavities scale. The crack tip propagates intermittently, through the coalescence of the cavities. This makes the effective crack tip velocities measured at the continuum scale much larger than the actual velocities measured at the cavity scale.

distances are found to be equal to $\delta_n = 115$ nm and $\delta_c = 168$ nm respectively, i.e. one order of magnitude larger than the values reported in Célarié et al. (2003a) concerning an aluminosilicate glass in similar experimental conditions, and consequently similar crack tip velocities at the continuous scale.

5. Discussion

The experiments reported in this paper reveal the existence of damage cavities in pure amorphous silica, qualitatively similar to the ones observed in an aluminosilicate glass (Célarié et al., 2003a). At the microscopic scale, the crack tip does not propagate regularly, but through the growth and coalescence of these cavities. It is worth mentioning that the chemical composition of silica is very simple. The observation of a nanoductile mode in such a "minimal" glass strongly indicates that the existence of this nanoductile mode is inherent to the amorphous structure and does not depend on the precise glass composition. This leads us to think that the scenario observed in MD simulations of dynamic fractures (Van Brutzel et al., 2002; Rountree et al., 2002) (very high velocities around the kilometer per second) can be extended to the stress corrosion regime: The amorphous structure results in toughness fluctuations at the nanoscale. The low toughness regions behave as stress concentrators and grow under the stress imposed by the main crack to give birth to the observed damage cavities.

However, it should be emphasized that the damage extension depends significantly on the glass composition. The cavity size at coalescence, 125 nm in the present experiment for pure silica (Fig. 5), was found to be around 20 nm in the aluminosilicate specimens for a similar loading configuration and a similar macroscopic crack front velocity. This confirms the importance of the chemical composition in the quantitative characteristics of the fracture process at the microscopic scale, as already pointed out by MD simulations (Van Brutzel, 1999; Van Brutzel et al., 2002; Falk and Langer, 2000). Complementary analysis addressing such questions are underway.

As already mentioned in Célarié et al. (2003a), the existence of a damaged zone explains the departure from linear elasticity observed in the vicinity of a stress corrosion crack tip (Guilloteau et al., 1996; Hénaux and Creuzet, 2000) in vitreous materials as well as the striking similarity between the morphologies of fracture surfaces in glass and metallic alloys (Daguier et al., 1997; Bouchaud, 1997) at different scales. In both types of materials, the crack progresses through the nucleation, growth and coalescence of damage cavities. These latter should thus be printed in the post-mortem fracture surface (Bouchaud and Paun, 1999). Consequently, their size should set the range of the different self-affine regimes observed on the fracture surface, leading to crossover lengths of a few tens nanometers in glass and a few hundreds micrometers in metallic

alloys, in good agreement to what was reported in Daguier et al. (1997). However it should be noted that our investigations are performed on the sample surface while the fracture surface morphology is related to the fracture of bulk. Investigation on the 3D distribution of the damage cavities in Silica are currently under progress.

Furthermore, in the classical ductile fracture mode of metallic materials, the crack tip progresses only through its joining with the closest damage cavity ahead. In the observed case, the cavity growth toward the main crack tip proceeds more quickly than the progression of the main crack itself: $\langle v\rangle^{\mathrm{FF}}/\langle v\rangle^{\mathrm{CT}} \simeq 2.7$.

Finally, the fact that the crack tip velocity at the continuum scale is significantly higher than the velocities of the different fronts (main crack, frontward and backward cavity tips) at the microscopic scale has important consequences on the relevance of classical stress corrosion models at ultra-slow crack propagation. Between the atomic scale and the continuum scale, there is an intermediate scale, the cavity scale, the dynamics of which should be taken into account, and become dominant for ultra-slow velocity. Consequently, it would be interesting to investigate the influence of the continuous velocity on the dynamics of the objects (main crack, cavities) at the intermediate scale. It may shed light onto the physical origin of the static limit (Wiederhorn, 1967; Wiederhorn and Bolz, 1970). Work in this direction is currently in progress.

Acknowledgment

We acknowledge Thierry Bernard for his technical support. We are also indebted to Fabrice Célarié, Rajiv Kalia, Christian Marlière, Mark Kachanov, Laurent Van Brutzel, and Sheldon Wiederhorn for enlightning discussions, and to Jean-Marc Cavedon and Georges Lozes for their constant support.

References

Bouchaud, E., 1997. Scaling properties of cracks. Journal of Physics: Condensed Matter 9 (21), 4319–4344 (and references therein).

Bouchaud, E., Paun, F., 1999. Fracture and damage at a microstructural scale. Computing in Science and Engineering 1 (5), 32–38.

Célarié, F., Prades, S., Bonamy, D., Ferrero, L., Bouchaud, E., Guillot, C., Marliere, C., 2003a. Glass breaks like metal, but at the nanometer scale. Physical Review Letters 90 (7), 075504/1-4.

Célarié, F., Prades, S., Bonamy, D., Dickele, A., Bouchaud, E., Guillot, C., Marliere, C., 2003b. Surface fracture of glassy materials as detected by real-time atomic force microscopy (AFM) experiments. Applied Surface Science 212, 92–96.

Daguier, P., Nghiem, B., Bouchaud, E., Creuzet, F., 1997. Pinning and depinning of crack fronts in heterogeneous materials. Physical Review Letters 78 (6), 1062–1065.

Falk, M.L., Langer, J.S., 2000. From simulation to theory in the physics of deformation and fracture. MRS Bulletin 25 (5), 40–45.

Guin, J.P., Wiederhorn, S.M., 2003. Crack growth threshold in soda lime silicate glass: role of hold-time. Journal of Non-Crystalline Solids 316 (1), 12–20.

Guilloteau, E., Charrue, H., Creuzet, F., 1996. The direct observation of the core region of a propagating fracture crack in glass. Europhysics Letters 34 (7), 549–553.

Hénaux, S., Creuzet, F., 2000. Crack tip morphology of slowly growing cracks in glass. Journal of the American Ceramic Society 83 (2), 415–417.

He, M.Y., Turner, M.R., Evans, A.G., 1995. Analysis of the double cleavage drilled compression specimen for interface fracture energy measurements over range of mode mixities. Acta Metallurgica Materialia 43, 3453–3458.

Kobayashi, T., Shockey, D.A., 1987. A fractographic investigation of thermal embrittlement in cast duplex stainless steel. Metallalurgical Transactions A 18A, 1941–1949.

Lawn, B.R., 1993. Fracture of Brittle Solids, second ed. Cambridge University Press, Cambridge.

Marlière, C., Prades, S., Célarié, F., Dalmas, D., Bonamy, D., Guillot, C., Bouchaud, E., 2003. Crack fronts and damage in glass at the nanometre scale. Journal of Physics: Condensed Matter 15 (31), 2377–2386.

Mandelbrot, B.B., Passoja, D.E., Paullay, A.J., 1984. Fractal character of fracture surfaces of metals. Nature 308, 721–722.

Pineau, A., François, D., Zaoui, A., 1995. Comportement Mécanique des Matériaux. Hermès, Paris.

Rice, J.M., Tracey, D.M., 1969. On the ductile enlargement of voids in triaxial stress fields. Journal of the Mechanics and Physics of Solids 17, 201–217.

Rountree, C.L., Kalia, R.K., Lidorikis, E., Nakano, A., Van Brutzel, L., Vashishta, P., 2002. Atomistic aspects of crack propagation in brittle materials: multimillion atom molecular dynamics simulations. Annual Review of Material Research 32, 377–400.

Van Brutzel, L., 1999. Contribution à L'etude des mécanismes de rupture dans les amorphes: étude par dynamique moléculaire de la rupture de verre de silice. Ph.D. thesis, Université Paris VI.

Van Brutzel, L., Rountree, C.L., Kalia, R.K., Nakano, A., Vashishta, P., 2002. Dynamic fracture mechanisms in nanostructured and amorphous silica glasses: million-atom molecular dynamics simulations. Materials Research Society Symposium Proceedings 703, V.3.9.1–V.3.9.6.

Wiederhorn, S.M., 1967. Influence of water vapor on crack propagation in Soda-lime glass. Journal of the American Ceramic Society 50, 407–414.

Wiederhorn, S.M., Bolz, L.H., 1970. Stress corrosion and static fatigue of glass. Journal of the American Ceramic Society 53, 543–548.